Preprint of the: Fabró, F., J. Montanyà, N. Pineda, O. Argemí, O. A. van der Velde, D. Romero, and S. Soula (2016), Analysis of energetic radiation associated with thunderstorms in the Ebro delta region in Spain, J. Geophys. Res. Atmos., 121, doi:10.1002/2015JD024573.

Analysis of energetic radiation associated with thunderstorms in the Ebro delta region in Spain

Ferran Fabró[1], Joan Montanyà[1], Nicolau Pineda[2], Oriol Argemí[2], Oscar A. van der Velde[1], David Romero[1], Serge Soula[3]

Corresponding author: F. Fabró, Department of Electrical Enginnering, Polytechnical University of Catalonia, Building TR1, Terrassa 08222, Barcelona, Spain. (ferran.fabro@upc.edu)

[1]Electrical Engineering Department,
Universitat Politècnica de Catalunya,
Barcelona, Spain.

[2]Meteorological Service of Catalonia,
Barcelona, Spain

[3]Laboratoire dAérologie, Université de
Toulouse, CNRS, Toulouse, France

Key Points.

- Background radiation during thunderstorms
- Radiation emitted by radon-ion daughters
- Experimental evidences of possible TGE detected

Abstract. The analysis of high-energy background radiation (0.1-2MeV) enhancements during eight winter thunderstorms and five summer storms in the Ebro delta region in the northeast of Spain is presented. For the first time, high-energy radiation counts, precipitation, radar reflectivity and very high frequency lightning detections to infer charge regions altitude have been analysed in order to find out what produces the measured background radiation increments associated with storms. The good agreement between radar reflectivity and precipitation with increases in background radiation counts coupled with the spectrum analysis comparing rain/no rain periods suggests that radon-ion daughters play a major role in the radiation increments reported. No evidence has been found supporting that measured background radiation enhancements can be produced by storm electric fields. Finally, a single case of a high energy radiation increase was prior to a cloud-to-ground lightning stroke which reinforces the theory of a lower positive charge layer to exist is important for the production of Terrestrial Ground Enhancements (TGEs).

1. Introduction

Since Wilson [1925] predicted that very energetic electrons within thunderstorm electric fields would be accelerated up to GeV energies, different experiments have shown that bursts of high-energy radiation occur inside thunderstorms. It is thought that those bursts are produced by the mechanism known as Relativistic Runaway Electron Avalanche (RREA), first introduced by Gurevich et al. [1992]. Referring to this mechanism, if the electrons (so called seed electrons) within an electric field are enough energetic to overcome the frictional force, they are accelerated up to relativistic energies. These relativistic electrons collide with air molecules producing new ones, leading to an avalanche of relativistic electrons that produce bursts of high energy radiation by Bremsstrahlung effect. Two different theories are proposed to explain the origin of the seed electrons.

The first one suggests that the seed electrons would be produced in the very high electric fields in lightning leader tips [Dwyer, 2008, 2010; Carlson et al., 2009, 2010; Celestin and Pasko, 2011] by the process known as cold runaway [Gurevich, 1961; Dwyer et al., 2004]. This mechanism would explain the bursts lasting milliseconds or less, generally observed in association with lightning that can be divided in two categories. The first one are the Terrestrial Gamma ray Flashes (TGFs) discovered by Fishman et al. [1994], detected in the upper atmosphere by instrumented satellites. Source altitude of TGFs is between 15 and 21 km [Dwyer and Smith, 2005; Carlson et al., 2007; Østgaard et al., 2008; Hazelton et al., 2009; Gjesteland et al., 2010] and they are thought to be produced by RREA of runaway electrons produced in the fronts of positive intra-cloud (IC) lightning leaders [Williams et al., 2006; Lu et al., 2010; Shao et al., 2010]. The second one are the X rays

detected at ground first observed by Moore et al. [2001]. In this case, the radiation has been detected in different situations like associated with leader steps of rocket triggered lightning [Dwyer et al., 2003], in multiple occasions associated with downward negative stepped leaders [Dwyer, 2005b; Howard et al., 2008; Saleh et al., 2009; Schaal et al., 2013; Mallick et al., 2012; Montanyà et al., 2014] and only in one case associated with upward leaders of both polarities [Yoshida et al., 2008]. It is thought that those X rays are produced by Bremsstrahlung effect of runaway electrons produced by cold runaway which is the same candidate process to explain X-rays in laboratory sparks [Dwyer, 2005a; Dwyer et al., 2008; Nguyen et al., 2008; March et al., 2009; March and Montanyà, 2010; Shao et al., 2011; Kochkin et al., 2012]. These very short-lasting events observed on ground detectors should be produced by negative IC lightning by the same mechanism as TGFs.

The second theory proposes that the seed electrons are secondary cosmic rays [Dwyer et al., 2003, 2008, 2012]. This theory is a very well proven phenomenon by the observation of the long TGEs, which are high energetic fluxes with durations of several seconds to several minutes and energies up to 10 MeV that seem to be modulated by the electric field of thunderstorms [Torii et al., 2009; Chilingarian et al., 2012]. Those events are often formed by γ radiation and energetic particles such as electrons and neutrons [Chilingarian et al., 2010]. Even if long TGEs have been observed in different situations, they have always been associated with thunderstorms. TGEs have been detected at altitudes above 2500 m [Torii et al., 2009; Tsuchiya et al., 2009; Chilingarian et al., 2011, 2012; Chilingarian and Mkrtchyan, 2012; Gurevich et al., 2013], at sea level associated only with winter thunderstorms [Torii et al., 2008, 2011], by balloons [Parks et al., 1981] and airplanes

[Eack et al., 1996]. Simulations [Babich and Loiko, 2010] have shown that long TGEs are produced inside tropospheric thunderclouds by RREAs of secondary cosmic rays with the source located at 0.5-2 km within the region between the main negative charge and the Lower Positive Charge Layer (LPCL), both for those observed at sea level and for those observed at mountain tops [Chilingarian, 2014].

On the other hand, Montanyà et al. [2014] reported the increment of high-energy counts clearly associated with precipitation (30 dBZ radar reflectivity) rather than storm electrification. This experiment was carried out on a mountain peak at 2500 m. The negative charge region was located near ~ 5.6 km, which is ~ 3 km above the detectors. Count rate increments were attributed to Radon (^{222}Rn and ^{220}Rn), i.e., radon-ion daughters, as also concluded by some other previous publications [Suszcynsky et al., 1996; Mallick et al., 2012]. Radon-ion daughters are products of the radiative decay chain of Uranium-238 (^{238}U) and Thoron-232 (^{232}Th). The existence of the increase of high energy radiation due to the radiative decay of radon-ion daughters during rain is a phenomenon that has been studied in great detail [Fujinami et al., 1985; Paatero and Hatakka, 1994; Vecchi et al., 2004; Takeyasu et al., 2006; Nayak et al., 2016].

The main aim of this paper is to find out if the high-energy background increments reported are long TGEs related to the storm electrification or to other factors like radiative decay of radon-ion daughters during precipitation. In order to achieve this objective we have analysed six episodes of high-energy radiation enhancements associated with storms divided in two groups, three days in winter and three days in summer, with eight winter storms and five summer storms identified. We present in section 2 the instruments used,

the methodology and the data analysed. Results are presented in section 3 and discussed in section 4. Finally, the main conclusions are summarized in section 5.

2. Instruments and data

Observations presented in this study were conducted in the Ebro delta region which is part of the so-called Ebro Valley Laboratory in the northeast of Spain. A specific instrument for the measurement of high-energy radiation was installed in the region in the specific location known as MonNatura, and has been in continuous operation from October 2013 to February 2015 (figure 1). This instrument consists of two ∅ 76 mm NaI(Tl)/photomultiplier tube scintillator detectors that are located within an aluminium box of 5 mm thickness wall to guarantee a good insulation of electromagnetic interference such as the intense electromagnetic fields produced by lightning. Both scintillators point upward behind two apertures covered by an aluminium foil of 1 mm. The first one is used to record transient high-energy radiation bursts associated with close lightning strikes. The second one is connected to the DP5G multichannel analyser of AMPTEK. This multichannel analyser is configured in the 1024 channels mode and is used to record cumulated counts of the high-energy background radiation in periods of 1 minute in the energy range 0.1-2 MeV. In this paper only the analysis of the background radiation detected by the second scintillator is carried out.

To have an estimation of the precipitation occurring on the high-energy instrument location, two data sources have been used. First, reflectivity data from the "Tivissa - Llaberia" (N 41° 05' 30.24"; E 0° 51' 48.58", 925 m) C-band single polarization Doppler weather radar operated by the Meteorological Service of Catalonia (SMC) is available every six minutes. In this paper time evolution of maximum value of the reflectivity

above the high-energy detector it is analysed. The 12-dBZ reflectivity threshold is used to identify rainy pixels. Moreover, by the analysis of radar images in the region, specifically images showing the Constant Altitude Plan Position Indicator (CAPPI) at 1 km (figure 2), time periods for each episode with convective cells over or very close to MonNatura have been identified. The threshold for convection has been taken as reflectivity $>$ 35 dBZ. Secondly, 10-min precipitation records were available from three Automatic Weather Stations (AWS, operated by the SMC) located in the vicinity of the instrument (figure 1). The precipitation in MonNatura has been estimated by interpolating the records of the three nearby AWS.

The region of the Ebro delta is very well covered by the VHF Ebro Lightning Mapping Array (ELMA) (figure 1), a total lightning three dimensional mapping network. It consists of 12 sensors that detect up to several thousands of VHF emissions of each flash [van der Velde and Montanyà, 2013]. As explained in the introduction, the existence of long TGEs is thought to be directly correlated with the existence of the LPCL. Therefore, LMA data has been used to infer the charge region altitudes above MonNatura. We proceeded using the same methodology as Pineda et al. [2016], but in this case taking into account only leaders above MonNatura over time intervals of ten minutes. This means that we are reporting only the specific charge regions that we can infer from LMA data. In order to differentiate between positive leaders and negative leaders, corresponding to negative charge and postive charge respectively, we have used the method developed by [van der Velde and Montanyà, 2013], a time-distance-altitude projection that helps to identify the leader polarity. We have also used LMA data to see if the storms analysed have electrical activity associated and yherefore can be considered thunderstorms (this is indicated in

the table 1). We have also used reanalysis data of ERA-Interim [Dee et al., 2011] together with outputs of the numerical prediction model Global Forecast System (GFS) in order to calculate the altitude of the isotherms 0°C, -10°C, -20°C, -40°C at 0000, 0600, 1200, 1800 and 2400 UTC for each one of the episodes at MonNatura location.

Figures 3 - 8 show the graphics for the six episodes analysed. In these figures, we present data in three different plots representing time evolution of variables presented above. The three graphics are the time evolution of high-energy radiation counts (a), rain (reflectivity, precipitation and convection, figures (b) and charge regions altitudes together with isotherms altitudes (c) for all the storms identified. High-energy counts have been filtered using 5-point local linear regression with first degree polynomial model in order remove false surges in counts that appear from time to time and are due to switching disturbances in the power supply.

Storms occurring during each episode have been identified using the graphics presented above. To have a better picture of the relation between radiation, reflectivity and precipitation, we have calculated the time difference between the beginnings of the radiation enhancement, 10 % above the background, and that of the precipitation (reflectivity) we name T10P (T10R). We calculate the same differences for the ends, when returning to 10 % above the background, T90P (T90R) for precipitation (reflectivity). We have used the 12-dBZ threshold, indicated in the description of the radar data, for the reflectivity. If radiation enhancements are produced by radon-ion daughters, we should expect that radiation increment begins and finishes after precipitation, i.e., $T10 > 0$ and $T90 > 0$. Moreover, we should expect that radiation increments would last longer than precipitation because radon-ion daughters deposited over the detector continue continue to decay

and emit radiation for a long time after precipitation finishes. This can be understood in terms of the measurements reported as T90 > T10. The values of these time differences are reported in table 1. Figure 9 shows the energy spectrum, for the episode 30 July 2013, for two different periods of 1 hour, one with rain and the other one without rain. We show only this case as representative of all because the spectrum is quite similar for all the episodes.

3. Analysis of data

3.1. Winter Storms

The three winter cases analysed are 16 November 2013, 30 November 2013 and 18 January 2014. For the 16 November 2013 episode it is possible to see in the figures 3.a and 3.b that for the five storms, radiation enhancements coincides very well with radar reflectivity just above the detector and precipitation issued from the three close stations, but only the first one has electrical activity associate with it. Convection above MonNatura is discontinuous, but there is also good correlation with the radiation increments. In figure 4.c it is shown that from 0900 to 0920 UTC (in Spain the LST is UTC+1 in winter and UTC+2 in summer) positive charge was present between 1.5 km and 3.6 km and negative charge from 3.5 km to 5.5 km only for the first storm. In table 1 can be seen that T10R > 0, T90R > 0 and T90P > 0 for all the cases. For the thunderstorms 1 and 3 T10P < 0.

For the case of 30 November 2013 it can be seen in the table 1 that T10R is 52 minutes and T10P is 18 minutes while T90R is 123 minutes and T90P is 127 minutes. This means that the radiation increment began 18 minutes after precipitation started and finished 127 minutes after precipitation ceased, that is 109 minutes longer than for the radiation curve. There is good agreement between reflectivity, precipitation and radiation increase (figures

4.a,b). However, in this case there is no lightning activity close enough to MonNatura to allow the inference of charge regions altitudes (figure 3.c). For this case the spectrum of two periods of one hour corresponding to rain and no-rain situations in the figure 9 it is also presented. The peaks 1 to 5 and 7 that exist only in the rainy period corresponds to radon-ion daughter decay energies, while the peak 6 that exists in both cases corresponds to potassium, as can be seen in the table 2. As previously mentioned, only one spectrum is presented because same peaks appear in the six episodes.

The last winter case, the 18 January 2014 episode, it has two identified storms (figure) between 0600 and 0800 UTC in the morning. For the first storm there is a good agreement between radiation and reflectivity increases but there was not convection (radar reflectivity below 35 dBZ, figures 4.a,b) and T10R >0, T90R >0 and T90R >T10R (table 1). Only the second one can be considered a thunderstorm, but no charge regions altitudes have been found (figures 4.c). For the second thunderstorm it can be observed in the figures 5.a and 5.b that convection exists and there is a clear agreement between radiation increase, reflectivity and precipitation. Table 1 shows that T10R is 17 minutes and T10P is 9 minutes while T90R is 71 minutes and T90P is 88 minutes, that is T10R >0, T90R >0, T90R >T10R and T10P >0, T90P >0, T90P >T10P.

3.2. Summer Storms

The first analysed day of summer is the 2 August 2014. Two storms have been identified. In figures 6.a and 6.b it can be seen that there is a good agreement between radiation increment and precipitation curves with a clear time delay of the radiation increment with respect to precipitation and there is only convection for the second one. Only the first storm has electrical activity associated (table 1). We have identified charge regions for

this thunderstorm, specifically positive charge regions (figure 6.c). It seems that these positive charge regions have different altitudes in two different periods, from 1220 to 1510 UTC between 5.5 and 10.3 km and from 1600 to 1730 UTC between 4 and 7.5 km. Table 1 shows that for both storms T10R, T90R, T10P and T90P are > 0 and only for the first case T90R $<$ T10R.

For the case of 20 August 2014 there are two storms identified (figure 7.a). For the first storm there is no lightning activity associated. In the table 1 we can see that radiation increment begins 85 minutes before precipitation starts (T10R = -85 minutes < 0) while radiation deceases 55 minutes after reflectivity ends (T90R = 55 minutes > 0), what means that T90R $>$ T10R, but no precipitations data exists. For the second storm identified radiation begins and ends after the reflectivity and precipitation(T10R and T10P are $>$ 0 and T90R and T90P > 0) and radiation increment lasts longer than reflectivity and precipitation (T90R $>$ T10R and T90P $>$ T10P). Figure 7.b shows that there is convective radar reflectivity for the second storm for which it has also been identified negative charge between 3.7 km and 5.8 km and positive charge between 7.8 km and 9.2 km.

Finally, for the case of 29 August 2014, there is one storm lasting less than one hour. There is a good agreement between reflectivity, precipitation and radiation (figures 8.a,b) and exists convective radar reflectivity. It can also be seen in table 1, as in most of the previous cases, that reflectivity and precipitation begin before a radiation increase, and decrease before the end of radiation (T10R $>$0, T90R $>$0, T10P $>$0 and T90P $>$0). Radiation enhancements have a longer duration than precipitation and reflectivity (T90R $>$T10R and T90P $>$T10P). Positive charge was identified between 3.5 km and 5.4 km and negative charge between 5 km and 7 km and between 8.5 km and 10 km (figure 8.c).

3.3. Single transient event

During the spring and summer of 2011 and 2012 the instrument was installed at the Eagle Nest instrumented tower (2537 m ASL) in the Spanish Pyrenees [Montanyà et al., 2014]. Here we present a single event recorded on . Electric field and high energy detections are depicted in figure 10.b. A - 93 kA CG impact struck 3.5 km from the instrument and 70 ms after the stroke an upward negative leader appeared from the top of the instrumented tower (figure 10.a). During this period the flash was very active within the cloud (figure 10.a). Note the high number of high energy detections at the beginning of the recording that significantly decreased at the time of the upward leader (t=0 ms). This type of case is unusual since upward negative leaders require negative electric fields meaning positive charge just above the tower. The reduction of the high energy count rates at the time of the upward leader would mean the reduction of the electric field between the main negative charge region and the positive charge above the tower. The isotherms have been calculated using ERA-Interim data and meteorological sounding in Barcelona.

4. Discussion

A total number of 13 storms have been identified, 8 in winter and and 5 in summer. Three winter storms and three summer storms have been classified as electrified thunderstorms, while the remaining seven storms do not have associated electric activity and cannot be considered thunderstorms (table 1). The analysis of the comparison of the spectra during rain/no rain periods (figure 9) shows peaks in the energy range of the radon-ion daughters which appear during rain periods. ^{222}Rn and ^{220}Rn are isotopes of radon descendants of ^{238}U and ^{232}Th created in the ground and spread into the troposphere. Both radon isotopes decay in solid radiative elements known as radon-ion daughters that can

be attached to water droplets when they precipitate. These radon-ion daughters can fall down above detectors during rain and then decay by α or β emissions. Radon-ion daughters are usually excited after the decay, what results in a γ emission that can be detected by high-energy detectors (see Bhandari [1963] for an extended explanation of radon-ion daughters). The NaI(Tl) scicntillator used to detect high-energy background radiation operates in the energy range from 0.1 to 2 MeV. Radon-ion daughters emit energies in the range from 0.1 MeV to 3 MeV [Yamazaki et al., 2002], which means that it is not easy to discern if radiation increments reported are due to radon-ion daughters or other factors. However, the spectra of figure 9 show that radon increment is mainly due to radon-ion daughters listed in table 2. We can see that 5 of them are descendants of ^{222}Rn while only one is a descendant of ^{220}Rn. That makes sense because although both radon isotopes have similar concentration in the atmosphere, half-life of ^{222}Rn is about 4 days while half-live of ^{220}Rn is about 56 seconds (from *Toxicological profile for radon*, 1990, by the Agency for Toxic Substances and Disease Registry of the U.S. Public Health Service in collaboration with the U.S. Environmental Protection Agency). These spectra are comparable to the ones obtained by Takeyasu et al. [2006] and Nayak et al. [2016] who found energetic peaks associated to the ^{214}Pb and ^{214}Bi radon-ion daughters during rainy periods. As commented before, the spectra of the 13 storms is quite similar (this is why only one case is presented), however it is important to comment that the radon-ion daughters peaks are higher during winter cases. This result agrees with Vecchi et al. [2004], who found that radon concentrations have the highest values during winter season and the lowest values during summer season.

We have observed that for all the storms analysed there is a good relation between radiation and precipitation and radar reflectivity. No specific behaviour has been found for convective periods. The analysis of time differences (T10R, T90R, T10P and T90P) of the table 1 can be summarized in the following points:

• In all of the cases T90R and T90P are > 0, which means that radiation increment continues after precipitation ceases. This is consistent with attributing radiation increment to precipitation because radon-ion daughters continues decaying and emitting after precipitation ceases.

• In 12 storms T10R > 0 while in 9 episodes T10P > 0, which means that radiation incrase begins after precipitation. T10R and T10P comprise a wide range of time differences from 6 to 134 minutes. Bhandari [1963] showed that 50% of precipitated radon-ion daughters decay after 50 minutes. If radiation is emitted by radon-ion daughter, its increment should take some time to start because of half-life of radon-ion daughters, which is consistent with the results presented here. Moreover, in 10 and 9 storms respectively T90R $>$ T10R and T90P $>$ T10P, which means that radiation increase takes more time to cease than reflectivity and precipitation.

• In only three cases, the first one of 20 August 2014, T10R < 0, and the first and the third of 16 November 2013, T10P < 0 .This means that radiation increment begins before precipitation starts. That could be explained by the advection of radon-ion daughters due to wind, as suggested by Vecchi et al. [2004] and Takeyasu et al. [2006].

According to Chilingarian et al. [2011] (see figure 10 from Chilingarian et al. [2011]), we assume that if downward runaway electrons and subsequent long TGEs are produced, seed MeV electrons would be provided by the cosmic-ray showers, and source region where

runaway electrons are produced, would be just between the main negative charge region and LPCL. Moreover production altitudes of long TGEs, and therefore LPCL altitude must be close enough to the ground for photons to overcome atmospheric attenuation and reach the detectors in the ground. That might be the case on 7 June 2011 (figure 10), because the tower is located at the top of a mountain at 2537 m asl and the boundary between the assumed LPCL and the main negative region was estimated to be < 2 km above the tower [Krehbiel, 1986] (figure 11). This is consistent with Babich and Loiko [2010] who determined from the spectra of radiation detected by Tsuchiya et al. [2007] at sea level in the coast of Japan that γ ray source location is at 0.5 - 2 km. In the case of 7 June 2011 in figure 10 it is shown a very unusual case of an upward negative leader, for which the rate of X-rays pulses detected remarkably decay after a -CG struck (-70 ms) close to the tower inducing the upward negative leader (0 ms) from the tower. The occurrence of an upward negative leader is very unexpected [Montanyà et al., 2014] and it is indicative of the presence of intense positive charge above the tower (or intense electric field pointing downwards). Other scenarios like an electrical polarity inverted thunderstorm could also explain the initiation of the negative upward leaders at the tower, but in this situation the occurrence of -CG would be very low. Also it could be possible that the preceding -CG removed negative charge from the cloud and exposed the upper positive charge to the ground initiating the leader. However, -CG flashes strike very often close to the Eagle Nest tower, and as we pointed out previously, negative upward leaders from the tower are very rare. Therefore, we assume the existence of the LPCL. Figure 11 shows the assumed sequence of events to figure out the anomalous high X-ray activity observed until the moment of the negative leader initiated at the tower: 1) Before the leader was initiated

at the tower, runaway electrons accelerated toward the ground in the high electric field between the main negative charge region and the LPCL produced a TGE event. After, the main negative charge was reduced because of the -CG stroke and intra-cloud activity, what led to a decrease of the intensity of the electric between the main negative charge region and the LPCL. 2) The intensity of the electric field had been reduced and it was not enough high to sustain the TGE. The cloud was more positive [Krehbiel et al., 2008] and the intensity of the electric field between the ground and cloud base had increased what led to the initiation of the negative leader at the tower. 3) The TGE finished.

We have also calculated the altitudes of the 0°C, -10°C, -20°C and -40°C isotherms for each one of the episodes analysed. The LPCL, if it exists, is usually between the 0°C and -10°C isotherms. In the figures 3 - 5.c it is shown that for the winter cases the altitude of the 0°C isotherm is between 1.2 km and 2.1 km and the altitude of the -10°C isotherm is between 2.7 km and 4 km. For the summer cases the altitude of the 0°C isotherm is between 3.5 km and 4.2 km and the altitude of the -10°C isotherm is between 5.2 km and 6.1 km. For these summer cases, it seems quite difficult that Bremmstrahlung photons emitted by runaway electrons produced at those altitude could overcome atmospheric attenuation and reach the scintillator placed at sea level, but for the winter cases, the altitudes agree with those determined by Babich and Loiko [2010]. In other publications γ ray sources have been located at lower altitudes: 60-130m [Tsuchiya et al., 2009], 700m [Tsuchiya et al., 2011] and 130 m [Chilingarian et al., 2010]. That indicates that the altitude of LPCL and source regions of long TGEs may be below 2 km. We have only determined positive charge at those altitudes, specifically between 1.5 and 3.5 km, during 20 minutes of the first storm of 16 November 2013 (figure 3.c) and during 10 minutes

of the second storm of 18 January 2014 (figure 5.c), but there was not any associated radiation increase different than that associated with the precipitation for either episodes.

Finally, it is important to say that the detectors used on these experiments detects photons with energies up to 10 MeV, which have a larger mean free path than radiation reported here (up to 2 MeV). This is the reason why, although radiation increments have been attributed to radon-ion daughters for the reasons discussed above, the possibility can not be rejected that NaI(Tl) scintillator is also being radiated by γ energetic photons produced by other mechanisms, like ~~long~~ TGEs.

5. Conclusions

We presented data of high-energy radiation enhancements with long durations associated with storms. The comparison of the energy spectra of rain/no rain periods together with the analysis of the time plots of radiation counts, radar reflectivity and precipitation leads us to conclude that the measured high-energy radiation enhancements are associated with radon-ion daughters rather than storm electrical activity. No difference have been found between electrified storms and non-electrified storms. Moreover, during 20 and 10 minutes respectively of two winter storms LPCL has been calculated to be between 1.5 km and 3.5 km, which could be enough for the photons produced at those altitudes by Bremmstrahlung effect to overcome atmospheric attenuation and reach the scintillator placed at sea level, but no association has been found. In order to observe high-energy radiation associated with storm electrifcation from ground, the negative charge region has to be very close to the ground, as in Japan winter coastal storms or high mountain observatories. These conditions are accomplished for the single case presented here from 7 June 2011, for which the occurrence of negative upward leader indicates the existence

of LPCL additionally with the location of the instrument at the top of mountain at 2537 m asl. Despite these results, the use of a detector in an energy from 0.1 MeV to 2 Mev does not allow to completely exclude the possibility that part of the high-energy radiation measured should be related storm electrification. In a future experiment we will use, together with the current detector, another with a broader energy range.

Acknowledgments. This study was supported by research grants from the Spanish Ministry of Economy and Competitiveness (MINECO) and European Regional Development Fund (ERDF) AYA2009-14027-C05-05, AYA2011-29936-C05-04, ESP2013-48032-C5-3-R and ESP2015-69909-C5-5-R. We also thanks MonNatura and "Parc Natural del Delta de l'Ebre" for hosting LMA antennas and high energy detector. Data available upon request: ferran.fabro@upc.edu.

References

Babich, L. P., Loiko, T. V., apr 2010. Peculiarities of detecting pulses of runaway electrons and X-rays generated by high-voltage nanosecond discharges in open atmosphere. Plasma Physics Reports 36 (3), 263–270.

Bhandari, N., jul 1963. Study of atmospheric washout processes by means of radon decay products. Journal of Geophysical Research 68 (13), 3823–3826.

Carlson, B. E., Lehtinen, N. G., Inan, U. S., apr 2007. Constraints on terrestrial gamma ray flash production from satellite observation. Geophysical Research Letters 34 (8), L08809.

Carlson, B. E., Lehtinen, N. G., Inan, U. S., dec 2009. Terrestrial gamma ray flash production by lightning current pulses. Journal of Geophysical Research 114, A00E08.

Carlson, B. E., Lehtinen, N. G., Inan, U. S., oct 2010. Terrestrial gamma ray flash production by active lightning leader channels. Journal of Geophysical Research 115 (A10), A10324.

Celestin, S., Pasko, V. P., mar 2011. Energy and fluxes of thermal runaway electrons produced by exponential growth of streamers during the stepping of lightning leaders and in transient luminous events. Journal of Geophysical Research 116 (A3), A03315.

Chilingarian, A., jan 2014. Thunderstorm ground enhancementsModel and relation to lightning flashes. Journal of Atmospheric and Solar-Terrestrial Physics 107, 68–76.

Chilingarian, A., Bostanjyan, N., Vanyan, L., apr 2012. Neutron bursts associated with thunderstorms. Physical Review D 85 (8), 085017.

Chilingarian, A., Daryan, A., Arakelyan, K., Hovhannisyan, A., Mailyan, B., Melkumyan, L., Hovsepyan, G., Chilingaryan, S., Reymers, A., Vanyan, L., aug 2010. Ground-based observations of thunderstorm-correlated fluxes of high-energy electrons, gamma rays, and neutrons. Physical Review D 82 (4), 043009.

Chilingarian, A., Hovsepyan, G., Hovhannisyan, A., mar 2011. Particle bursts from thunderclouds: Natural particle accelerators above our heads. Physical Review D 83 (6), 062001.

Chilingarian, A., Mkrtchyan, H., oct 2012. Role of the Lower Positive Charge Region (LPCR) in initiation of the Thunderstorm Ground Enhancements (TGEs). Physical Review D 86 (7), 072003.

Dee, D. P., Uppala, S. M., Simmons, A. J., Berrisford, P., Poli, P., Kobayashi, S., Andrae, U., Balmaseda, M. A., Balsamo, G., Bauer, P., Bechtold, P., Beljaars, A. C. M., van de Berg, L., Bidlot, J., Bormann, N., Delsol, C., Dragani, R., Fuentes, M., Geer, A. J.,

Haimberger, L., Healy, S. B., Hersbach, H., Hólm, E. V., Isaksen, L., Kållberg, P., Köhler, M., Matricardi, M., McNally, A. P., Monge-Sanz, B. M., Morcrette, J.-J., Park, B.-K., Peubey, C., de Rosnay, P., Tavolato, C., Thépaut, J.-N., Vitart, F., apr 2011. The ERA-Interim reanalysis: configuration and performance of the data assimilation system. Quarterly Journal of the Royal Meteorological Society 137 (656), 553–597.

Dwyer, J. R., 2005a. The initiation of lightning by runaway air breakdown. Geophysical Research Letters 32 (20), L20808.

Dwyer, J. R., 2005b. X-ray bursts associated with leader steps in cloud-to-ground lightning. Geophysical Research Letters 32 (1), L01803.

Dwyer, J. R., may 2008. Source mechanisms of terrestrial gamma-ray flashes. Journal of Geophysical Research 113 (D10), D10103.

Dwyer, J. R., mar 2010. Diffusion of relativistic runaway electrons and implications for lightning initiation. Journal of Geophysical Research 115, A00E14.

Dwyer, J. R., Rassoul, H. K., Al-Dayeh, M., Caraway, L., Wright, B., Chrest, A., Uman, M. A., Rakov, V. A., Rambo, K. J., Jordan, D. M., Jerauld, J., Smyth, C., mar 2004. Measurements of x-ray emission from rocket-triggered lightning. Geophysical Research Letters 31 (5), n/a–n/a.

Dwyer, J. R., Saleh, Z., Rassoul, H. K., Concha, D., Rahman, M., Cooray, V., Jerauld, J., Uman, M. A., Rakov, V. A., dec 2008. A study of X-ray emission from laboratory sparks in air at atmospheric pressure. Journal of Geophysical Research 113 (D23), D23207.

Dwyer, J. R., Smith, D. M., 2005. A comparison between Monte Carlo simulations of runaway breakdown and terrestrial gamma-ray flash observations. Geophysical Research Letters 32 (22), L22804.

Dwyer, J. R., Smith, D. M., Cummer, S. A., jun 2012. High-Energy Atmospheric Physics: Terrestrial Gamma-Ray Flashes and Related Phenomena. Space Science Reviews 173 (1-4), 133–196.

Dwyer, J. R., Uman, M. A., Rassoul, H. K., Al-Dayeh, M., Caraway, L., Jerauld, J., Rakov, V. A., Jordan, D. M., Rambo, K. J., Corbin, V., Wright, B., jan 2003. Energetic radiation produced during rocket-triggered lightning. Science (New York, N.Y.) 299 (5607), 694–7.

Eack, K. B., Beasley, W. H., Rust, W. D., Marshall, T. C., Stolzenburg, M., dec 1996. Initial results from simultaneous observation of X-rays and electric fields in a thunderstorm. Journal of Geophysical Research 101 (D23), 29637.

Fishman, G. J., Bhat, P. N., Mallozzi, R., Horack, J. M., Koshut, T., Kouveliotou, C., Pendleton, G. N., Meegan, C. A., Wilson, R. B., Paciesas, W. S., Goodman, S. J., Christian, H. J., may 1994. Discovery of intense gamma-ray flashes of atmospheric origin. Science (New York, N.Y.) 264 (5163), 1313–6.

Fujinami, N., Esaka, S., Minato, S., jul 1985. Influence of the precipitation rate on the seasonal variation in the specific radioactivity of short-lived222Rn daughters in precipitation. Journal of Radioanalytical and Nuclear Chemistry Letters 95 (2), 111–117.

Gjesteland, T., Østgaard, N., Connell, P. H., Stadsnes, J., Fishman, G. J., may 2010. Effects of dead time losses on terrestrial gamma ray flash measurements with the Burst and Transient Source Experiment. Journal of Geophysical Research 115, A00E21.

Gurevich, A., nov 1961. ON THE THEORY OF RUNAWAY ELECTRONS. Soviet Phys. JETP 12(5), 904–912.

Gurevich, A., Milikh, G., Roussel-Dupre, R., jun 1992. Runaway electron mechanism of air breakdown and preconditioning during a thunderstorm. Physics Letters A 165 (5-6), 463–468.

Gurevich, A. V., Antonova, V. P., Chubenko, A. P., Karashtin, A. N., Mitko, G. G., Ptitsyn, M. O., Ryabov, V. A., Shepetov, A. L., Shlyugaev, Y. V., Vildanova, L. I., Zybin, K. P., feb 2013. Cosmic rays and thunderstorms at the Tien-Shan mountain station. Journal of Physics: Conference Series 409 (1), 012234.

Hazelton, B. J., Grefenstette, B. W., Smith, D. M., Dwyer, J. R., Shao, X.-M., Cummer, S. A., Chronis, T., Lay, E. H., Holzworth, R. H., jan 2009. Spectral dependence of terrestrial gamma-ray flashes on source distance. Geophysical Research Letters 36 (1), L01108.

Howard, J., Uman, M. A., Dwyer, J. R., Hill, D., Biagi, C., Saleh, Z., Jerauld, J., Rassoul, H. K., jul 2008. Co-location of lightning leader x-ray and electric field change sources. Geophysical Research Letters 35 (13), L13817.

Kochkin, P. O., Nguyen, C. V., van Deursen, A. P. J., Ebert, U., oct 2012. Experimental study of hard x-rays emitted from metre-scale positive discharges in air. Journal of Physics D: Applied Physics 45 (42), 425202.

Krehbiel, P. R., 1986. The electrical structure of thunderstorms, The Earth's Electrical Enviroment, Studies in Geophysics. National Academy Press, Washington D.C.

Krehbiel, P. R., Riousset, J. A., Pasko, V. P., Thomas, R. J., Rison, W., Stanley, M. A., Edens, H. E., apr 2008. Upward electrical discharges from thunderstorms. Nature Geoscience 1 (4), 233–237.

Lu, G., Blakeslee, R. J., Li, J., Smith, D. M., Shao, X.-M., McCaul, E. W., Buechler, D. E., Christian, H. J., Hall, J. M., Cummer, S. A., jun 2010. Lightning mapping observation of a terrestrial gamma-ray flash. Geophysical Research Letters 37 (11), n/a–n/a.

Mallick, S., Rakov, V. A., Dwyer, J. R., aug 2012. A study of X-ray emissions from thunderstorms with emphasis on subsequent strokes in natural lightning. Journal of Geophysical Research 117 (D16), D16107.

March, V., Arrayás, M., Trueba, J. L., Montanyà, J., Romero, D., Solà, G., Aranguren, D., may 2009. Features of electrical discharges in air triggered by laser. Journal of Electrostatics 67 (2-3), 301–306.

March, V., Montanyà, J., oct 2010. Influence of the voltage-time derivative in X-ray emission from laboratory sparks. Geophysical Research Letters 37 (19), n/a–n/a.

Montanyà, J., Fabró, F., van der Velde, O., Romero, D., Solà, G., Hermoso, J. R., Soula, S., Williams, E. R., Pineda, N., feb 2014. Registration of X-rays at 2500m altitude in association with lightning flashes and thunderstorms. Journal of Geophysical Research: Atmospheres 119 (3), 1492–1503.

Moore, C. B., Eack, K. B., Aulich, G. D., Rison, W., jun 2001. Energetic radiation associated with lightning stepped-leaders. Geophysical Research Letters 28 (11), 2141–2144.

Nayak, P., Gupta, S., Jain, A., Mazumdar, I., Raha, S., jan 2016. Study of terrestrial γ-ray background in presence of variable radioactivity from rain water. Astroparticle Physics 72, 55–60.

Nguyen, C. V., van Deursen, A. P. J., Ebert, U., dec 2008. Multiple x-ray bursts from long discharges in air. Journal of Physics D: Applied Physics 41 (23), 234012.

Østgaard, N., Gjesteland, T., Stadsnes, J., Connell, P. H., Carlson, B., feb 2008. Production altitude and time delays of the terrestrial gamma flashes: Revisiting the Burst and Transient Source Experiment spectra. Journal of Geophysical Research 113 (A2), A02307.

Paatero, J., Hatakka, J., 1994. No TitleWet deposition efficiency of short-lived radon-222 progeny in central Finland. BOREAL ENVIRONMENT RESEARCH 4, 285–293.

Parks, G. K., Mauk, B. H., Spiger, R., Chin, J., nov 1981. X-ray enhancements detected during thunderstorm and lightning activities. Geophysical Research Letters 8 (11), 1176–1179.

Pineda, N., Rigo, T., Montanyà, J., van der Velde, O. A., sep 2016. Charge structure analysis of a severe hailstorm with predominantly positive cloud-to-ground lightning. Atmospheric Research 178-179, 31–44.

Saleh, Z., Dwyer, J., Howard, J., Uman, M., Bakhtiari, M., Concha, D., Stapleton, M., Hill, D., Biagi, C., Rassoul, H., sep 2009. Properties of the X-ray emission from rocket-triggered lightning as measured by the Thunderstorm Energetic Radiation Array (TERA). Journal of Geophysical Research 114 (D17), D17210.

Schaal, M. M., Dwyer, J. R., Rassoul, H. K., Hill, J. D., Jordan, D. M., Uman, M. A., oct 2013. The angular distribution of energetic electron and X-ray emissions from triggered lightning leaders. Journal of Geophysical Research: Atmospheres 118 (20), 11,712–11,726.

Shao, T., Zhang, C., Niu, Z., Yan, P., Tarasenko, V. F., Baksht, E. K., Burahenko, A. G., Shut'ko, Y. V., jan 2011. Diffuse discharge, runaway electron, and x-ray in atmospheric pressure air in an inhomogeneous electrical field in repetitive pulsed modes. Applied

Physics Letters 98 (2), 021503.

Shao, X.-M., Hamlin, T., Smith, D. M., jun 2010. A closer examination of terrestrial gamma-ray flash-related lightning processes. Journal of Geophysical Research 115, A00E30.

Suszcynsky, D. M., Roussel-Dupre, R., Shaw, G., oct 1996. Ground-based search for X rays generated by thunderstorms and lightning. Journal of Geophysical Research 101 (D18), 23505.

Takeyasu, M., Iida, T., Tsujimoto, T., Yamasaki, K., Ogawa, Y., jan 2006. Concentrations and their ratio of (222)Rn decay products in rainwater measured by gamma-ray spectrometry using a low-background Ge detector. Journal of environmental radioactivity 88 (1), 74–89.

Torii, T., Sugita, T., Kamogawa, M., Watanabe, Y., Kusunoki, K., dec 2011. Migrating source of energetic radiation generated by thunderstorm activity. Geophysical Research Letters 38 (24), n/a–n/a.

Torii, T., Sugita, T., Muraki, Y., 2008. Observation of the gradual increases and bursts of energetic radiation associated with the activity of the winter thunderstorm.

Torii, T., Sugita, T., Tanabe, S., Kimura, Y., Kamogawa, M., Yajima, K., Yasuda, H., jul 2009. Gradual increase of energetic radiation associated with thunderstorm activity at the top of Mt. Fuji. Geophysical Research Letters 36 (13), L13804.

Tsuchiya, H., Enoto, T., Torii, T., Nakazawa, K., Yuasa, T., Torii, S., Fukuyama, T., Yamaguchi, T., Kato, H., Okano, M., Takita, M., Makishima, K., jun 2009. Observation of an Energetic Radiation Burst from Mountain-Top Thunderclouds. Physical Review Letters 102 (25), 255003.

Tsuchiya, H., Enoto, T., Yamada, S., Yuasa, T., Kawaharada, M., Kitaguchi, T., Kokubun, M., Kato, H., Okano, M., Nakamura, S., Makishima, K., oct 2007. Detection of High-Energy Gamma Rays from Winter Thunderclouds. Physical Review Letters 99 (16), 165002.

Tsuchiya, H., Enoto, T., Yamada, S., Yuasa, T., Nakazawa, K., Kitaguchi, T., Kawaharada, M., Kokubun, M., Kato, H., Okano, M., Makishima, K., may 2011. Long-duration γ ray emissions from 2007 and 2008 winter thunderstorms. Journal of Geophysical Research 116 (D9), D09113.

van der Velde, O. A., Montanyà, J., dec 2013. Asymmetries in bidirectional leader development of lightning flashes. Journal of Geophysical Research: Atmospheres 118 (24), 13,504–13,519.

Vecchi, R., Marcazzan, G., Valli, G., Ceriani, M., Antoniazzi, C., sep 2004. The role of atmospheric dispersion in the seasonal variation of PM1 and PM2.5 concentration and composition in the urban area of Milan (Italy). Atmospheric Environment 38 (27), 4437–4446.

Williams, E., Boldi, R., Bór, J., Sátori, G., Price, C., Greenberg, E., Takahashi, Y., Yamamoto, K., Matsudo, Y., Hobara, Y., Hayakawa, M., Chronis, T., Anagnostou, E., Smith, D. M., Lopez, L., 2006. Lightning flashes conducive to the production and escape of gamma radiation to space. Journal of Geophysical Research 111 (D16), D16209.

Wilson, C., oct 1925. The Acceleration of β-particles in Strong Electric Fields such as those of Thunderclouds. Mathematical Proceedings of the Cambridge Philosophical Society 22 (04), 534–538.

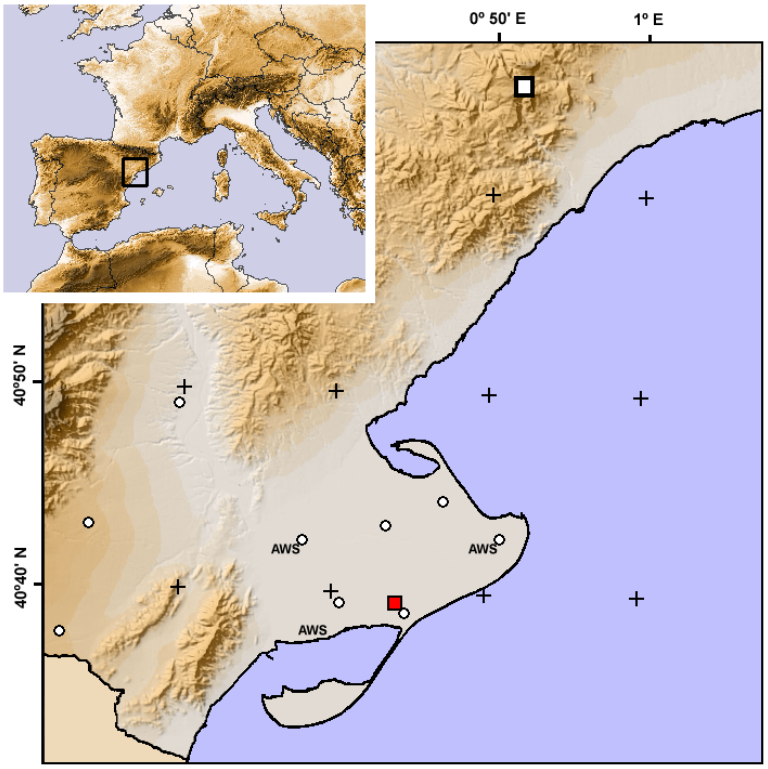

Figure 1. Location of the NaI(TL) scitillator (red aquare), automathic weather stations (AWS), LMA antennas (white circles) and radar (white square) in the Ebro delta in the north-east of Spain

Yamazaki, K., Tonouchi, S., Hashimoto, T., 2002. Factors associated with the variations in environmental gamma-ray spectra in Kashiwazaki Kariwa area. Journal of Radioanalytical and Nuclear Chemistry 252 (2), 359–366.

Yoshida, S., Morimoto, T., Ushio, T., Kawasaki, Z.-I., Torii, T., Wang, D., Takagi, N., Watanabe, T., may 2008. High energy photon and electron bursts associated with upward lightning strokes. Geophysical Research Letters 35 (10), L10804.

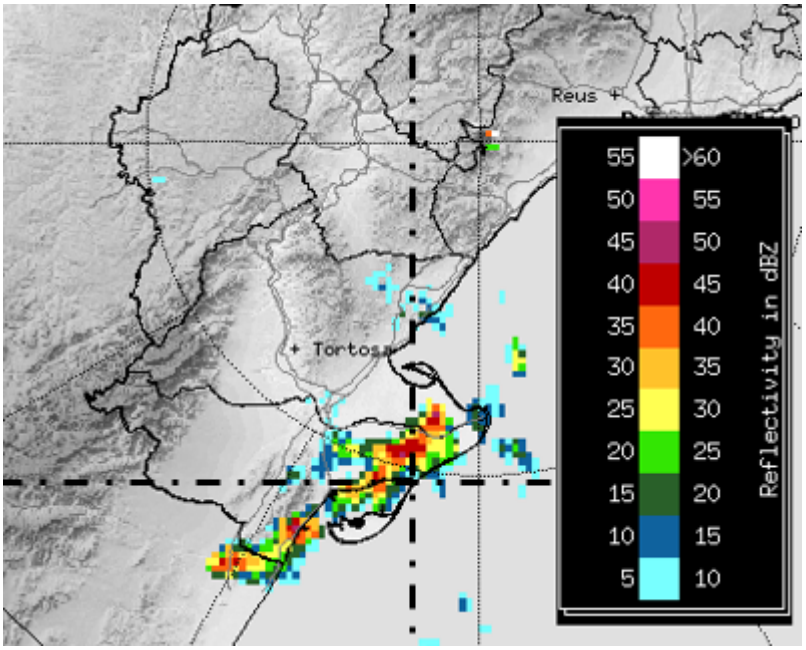

Figure 2. CAPPI at 1km for the 29 August 2014 at 0518 UTC. MonNatura location is in the intersection of the dot-dash lines

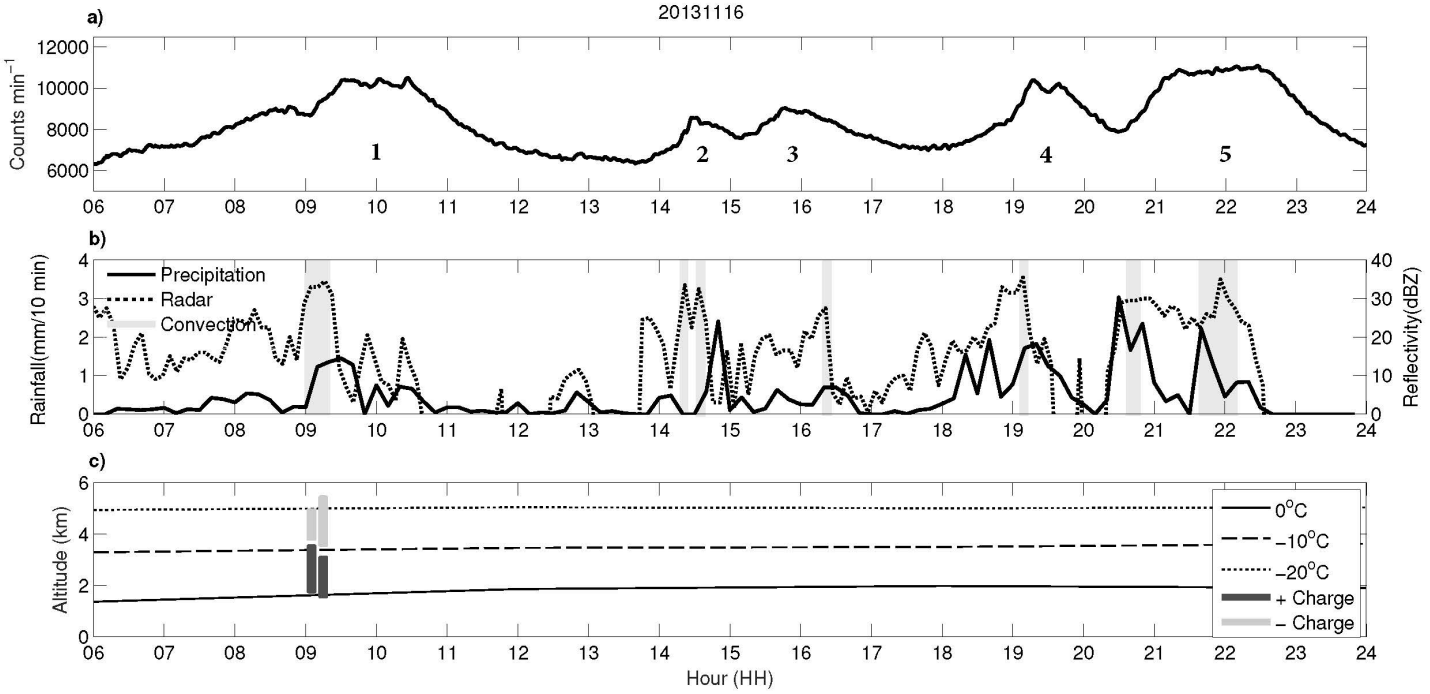

Figure 3. Time evolution for 30 November 2013 episode of (a) X ray counts, (b) maximum radar reflectivity and precipitation above the scintillator and (c) altitude of the 0°C, -10°C and -20°C isotherms charge regions altitudes inferred from LMA detections

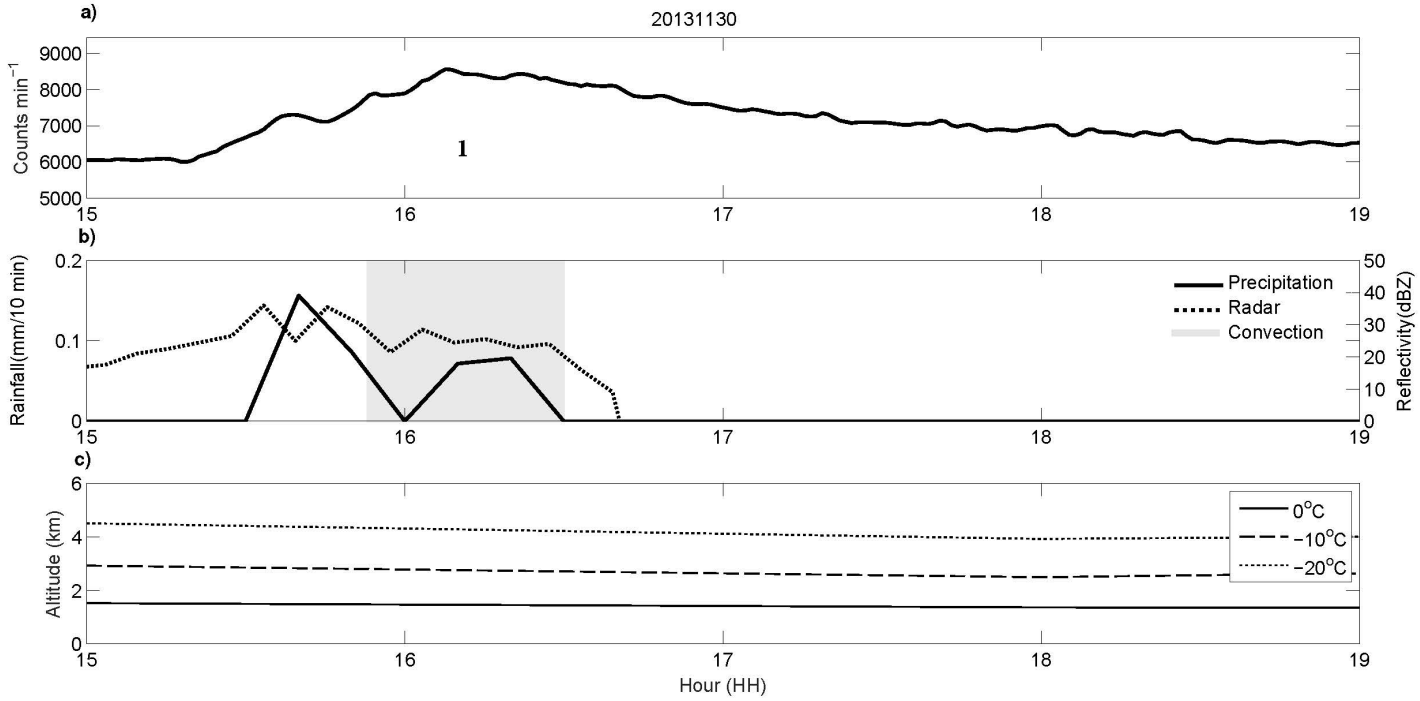

Figure 4. Time evolution for 30 November 2013 episode of (a) X ray counts, (b) maximum radar reflectivity and precipitation above the scintillator and (c) altitude of the 0°C, -10°C and -20°C isotherms charge regions altitudes inferred from LMA detections

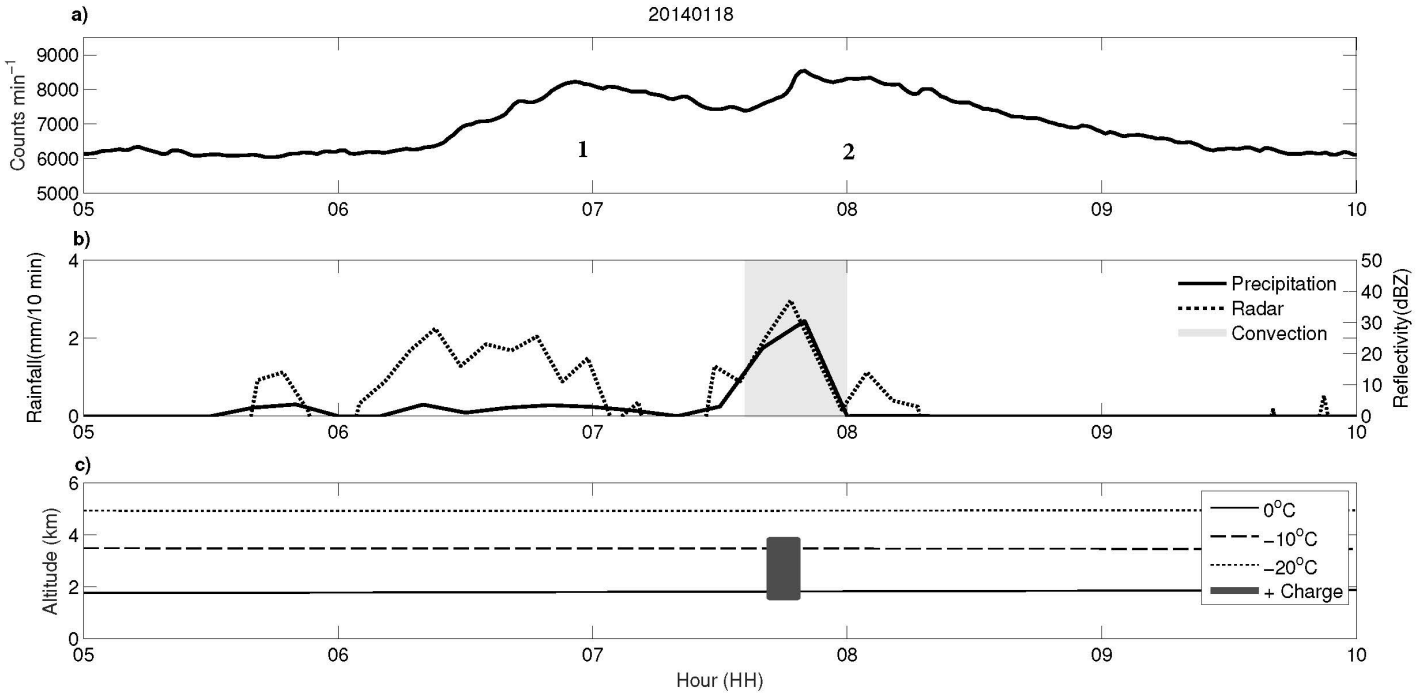

Figure 5. Time evolution for 18 January 2014 episode of (a) X ray counts, (b) maximum radar reflectivity and precipitation above the scintillator and (c) altitude of the 0°C, -10°C and -20°C isotherms charge regions altitudes inferred from LMA detections

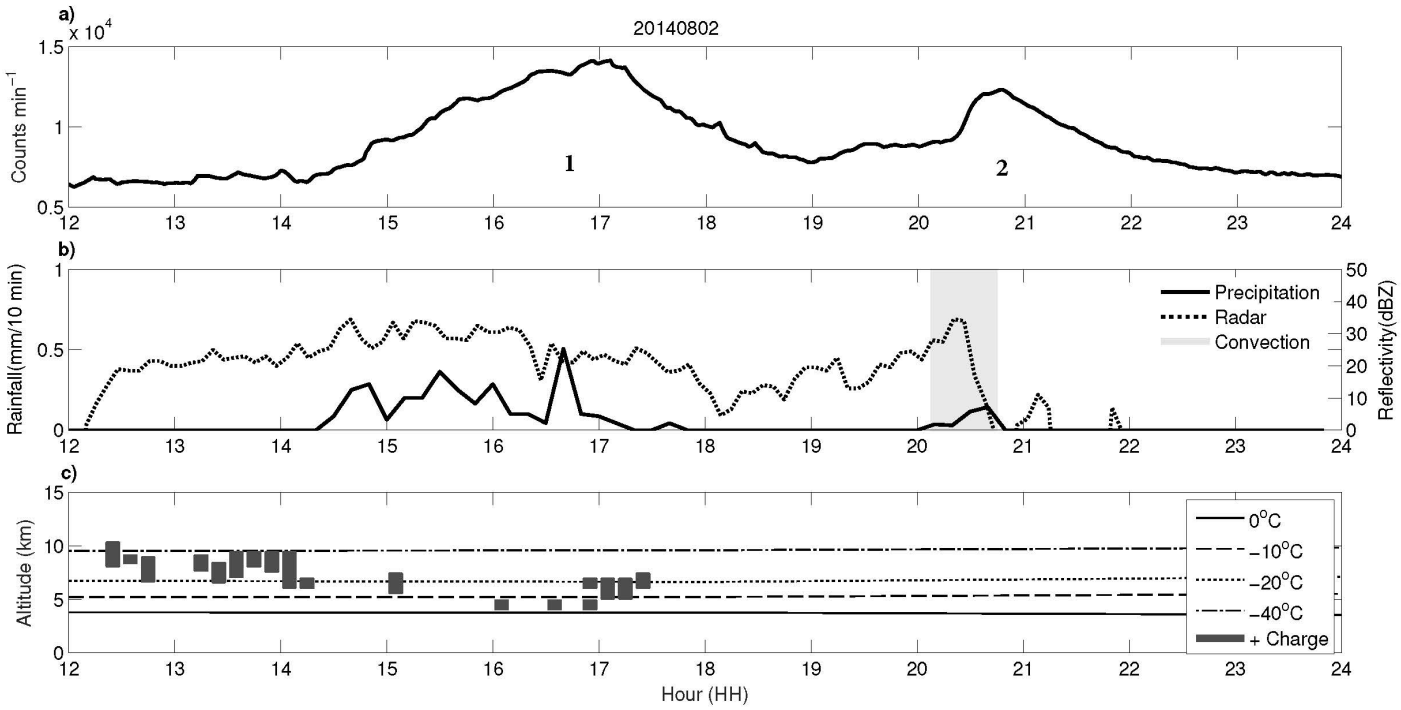

Figure 6. Time evolution for 2 August 2014 episode of (a) X ray counts, (b) maximum radar reflectivity and precipitation above the scintillator and (c) altitude of the 0°C, -10°C , -20°C and -40°C isotherms charge regions altitudes inferred from LMA detections

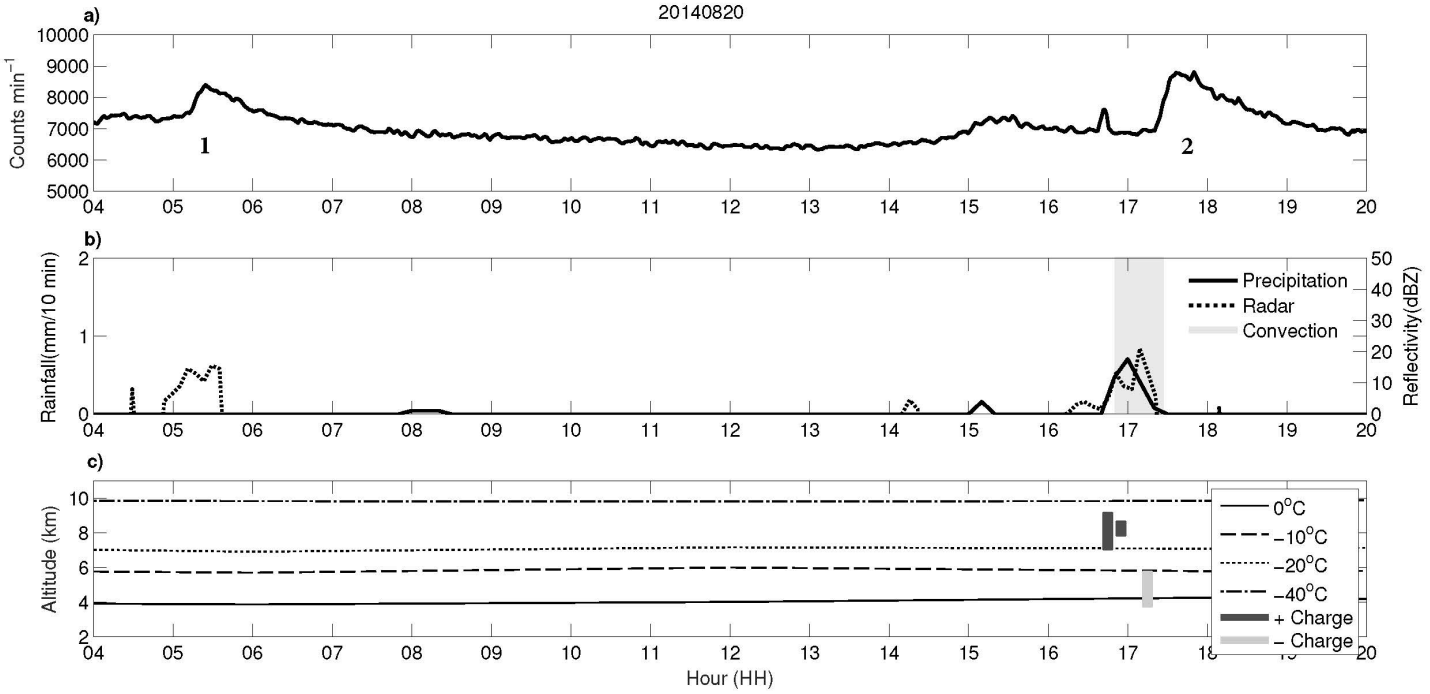

Figure 7. Time evolution for 20 August 2014 episode of (a) X ray counts, (b) maximum radar reflectivity and precipitation above the scintillator and (c) altitude of the 0°C, -10°C , -20°C and -40°C isotherms charge regions altitudes inferred from LMA detections

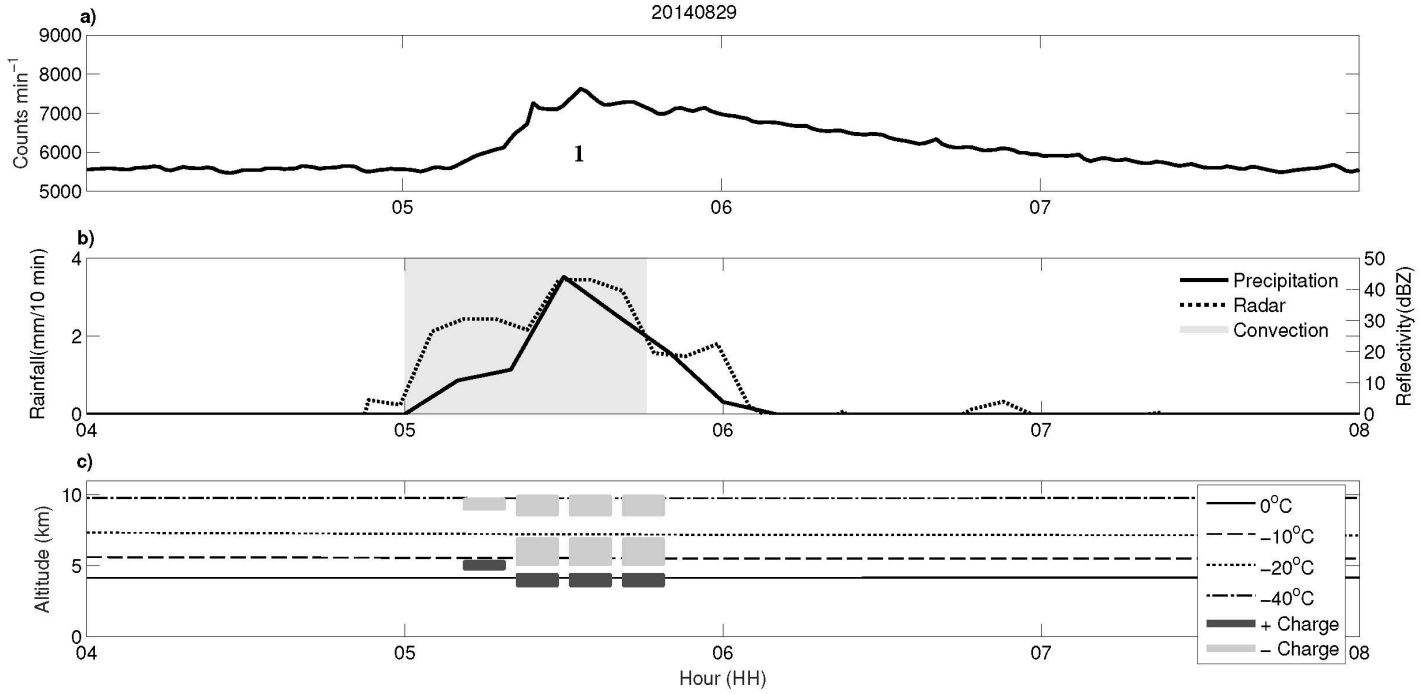

Figure 8. Time evolution for 29 August 2014 episode of (a) X ray counts, (b) maximum radar reflectivity and precipitation above the scintillator and (c) altitude of the 0°C, -10°C , -20°C and -40°C isotherms charge regions altitudes inferred from LMA detections

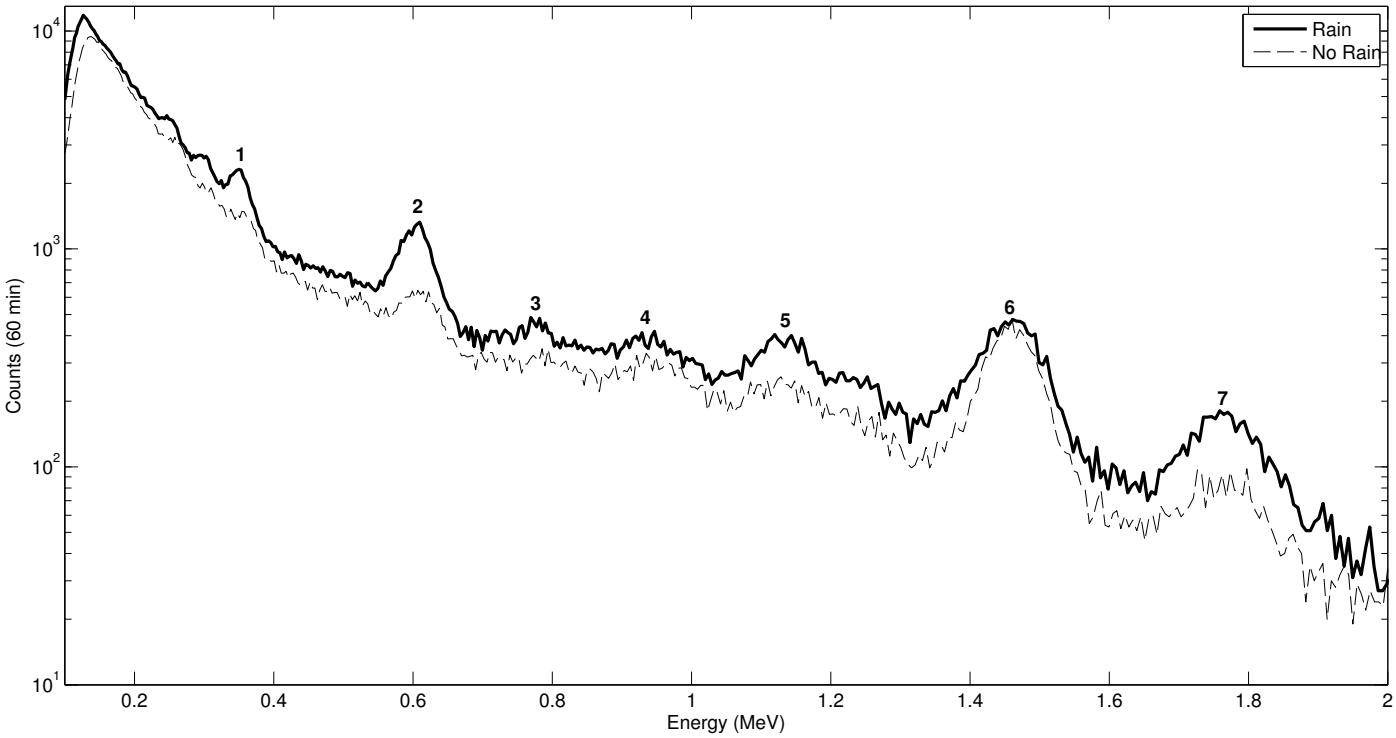

Figure 9. Energy spectra of 1 hour period with rain and 1 hour period without rain for the 30 November 2013 episode

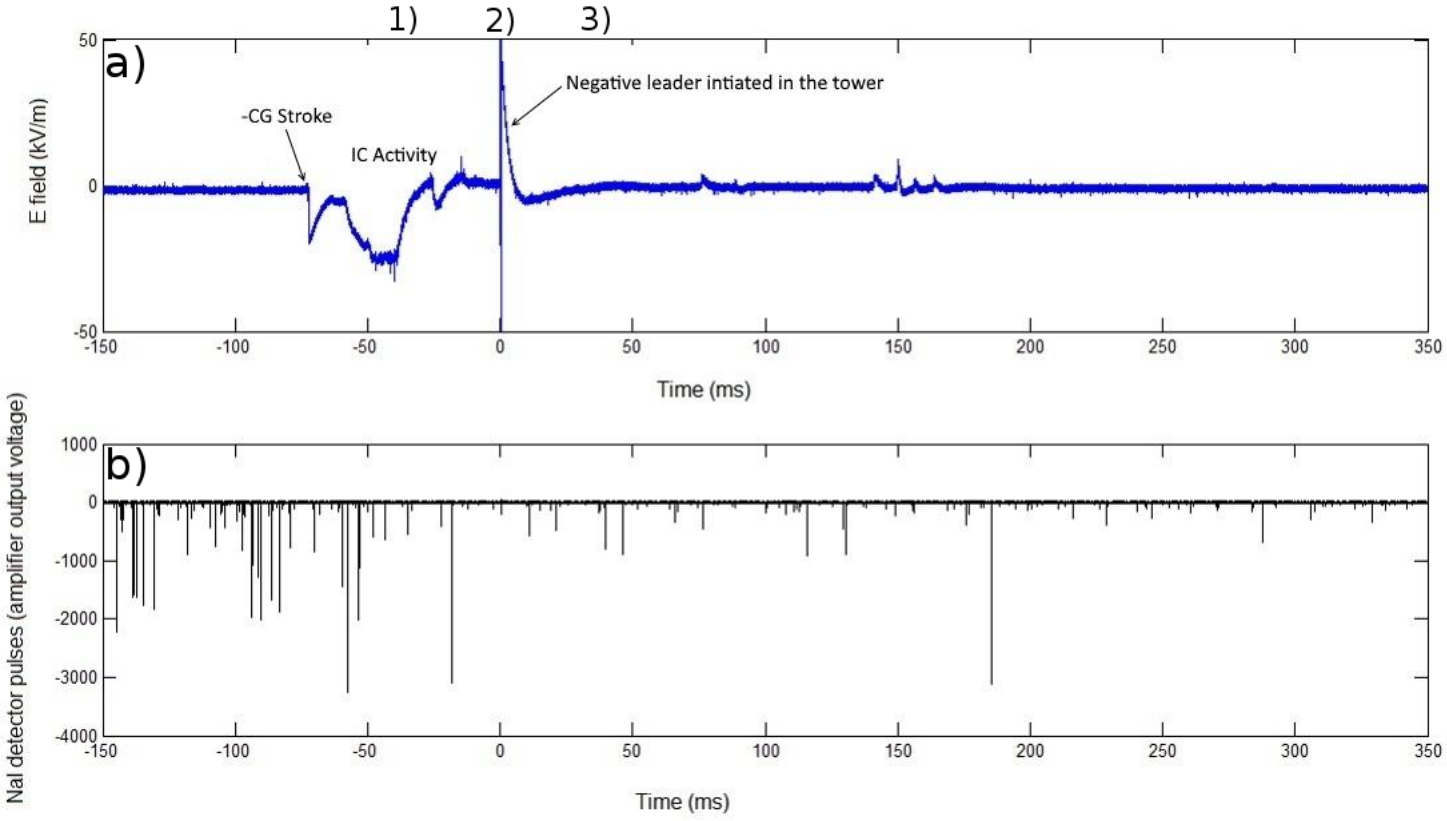

Figure 10. Case of the 7 June 2011. (a) Electric field of a CG stroke (-70 ms) at 3.5 km from the tower and occurrence of an upward negative leader from the tower (0 ms). (b) X-rays pulses. Note the decrease of the intense pulse rate after the occurrence of the downward negative CG (-70 ms) and the induced upward negative leader (0 ms). The number 1, 2 and 3 corresponds to the moments of the figure 11

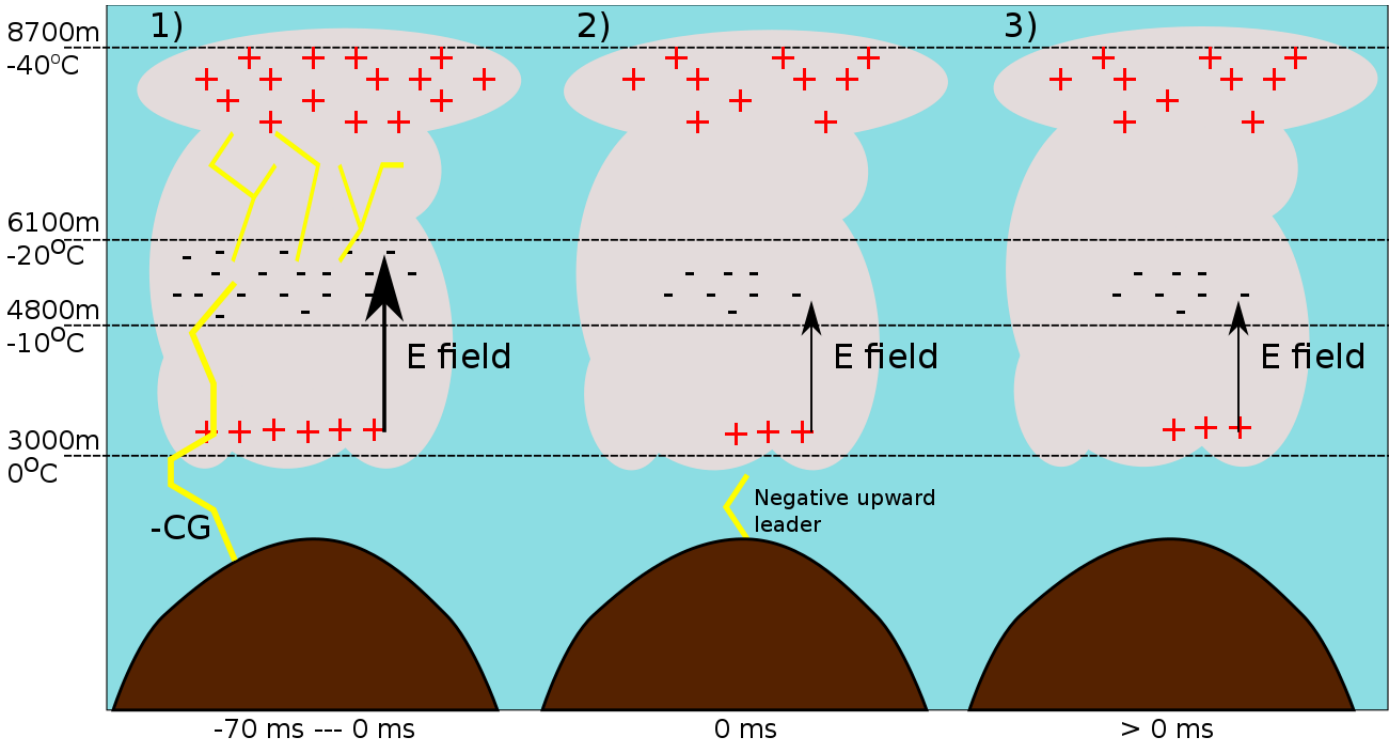

Figure 11. Case of 7 June 2011 occurring at the Eagle Nest tower at 2537 m asl. 1) Downward negative CG and and IC activity (t $<$ 0 ms). The intensity of the electric field between the LPCL and main negative charge region has been decreasing progressively until the occurrence of the 2) upward negative leader (t = 0 ms). 3) The intensity of the electric field is not enough high to sustain the TGE (t$>$ 0 ms).

Table 1. Time differences T10R, T90R, T10P and T90P of every one of the storms identified. The storm numbers in bold corresponds to thunderstorms.

	Day	Storm	T10R (min)	T90R (min)	T10P (min)	T90P (min)
Winter	20131116	**1**	99	101	-11	50
		2	16	19	10	1
		3	1.6	29	-14	20
		4	47	40	15	30
		5	16	55	27	73
	20131130	**1**	52	123	18	127
	20140118	1	9	28	-	-
		2	17	71	9	88
Summer	20140802	**1**	134	41	40	85
		2	87	123	12	113
	20140820	1	-85	55	-	-
		2	34	93	38	102
	20140829	**1**	6	54	8	58

Table 2. Energies of the peaks identified in the spectrum of figure 9 of potassium and those corresponding to radon-ion daughters descendants of decay chains of uranium and thorium. (Adapted from Yamazaki et al. [2002])

Peak	^{222}Rn (^{238}U Series) (MeV)	^{220}Rn (^{235}Th Series) (MeV)	^{40}K (MeV)
1	^{214}Pb (0.352)		
2	^{214}Bi (0.609)		
3	^{214}Bi (0.768)		
4		^{208}Tl (0.860)	
5	^{214}Bi (1.120)		
6			^{40}K (1.461)
7	^{214}Bi (1.764)		